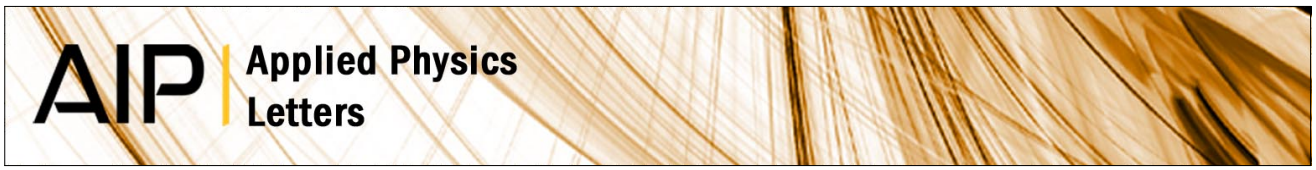

A bi-functional quantum cascade device for same-frequency lasing and detection

Benedikt Schwarz, Peter Reininger, Hermann Detz, Tobias Zederbauer, Aaron Maxwell Andrews et al.

Citation: Appl. Phys. Lett. **101**, 191109 (2012); doi: 10.1063/1.4767128
View online: http://dx.doi.org/10.1063/1.4767128
View Table of Contents: http://apl.aip.org/resource/1/APPLAB/v101/i19
Published by the AIP Publishing LLC.

A bi-functional quantum cascade device for same-frequency lasing and detection

Benedikt Schwarz,[1,a)] Peter Reininger,[1] Hermann Detz,[1] Tobias Zederbauer,[1] Aaron Maxwell Andrews,[1] Stefan Kalchmair,[1] Werner Schrenk,[1] Oskar Baumgartner,[2] Hans Kosina,[2] and Gottfried Strasser[1]
[1]*Institute for Solid State Electronics and Center for Micro- and Nanostructures, Vienna University of Technology, Vienna, Austria*
[2]*Institute for Microelectronics, Vienna University of Technology, Vienna, Austria*

(Received 18 October 2012; accepted 29 October 2012; published online 8 November 2012)

We demonstrate a bi-functional quantum cascade device that detects at the same wavelength as it coherently emits. Our fabricated device operates at room-temperature with a pulsed peak power emission of 45 mW and a detector responsivity of 3.6 mA/W. We show how to compensate the intrinsic wavelength mismatch between the laser and the detector, based on a bound-to-continuum design. An overlap between the laser and the detector spectra was observed from 6.4 μm to 6.8 μm. The electro-luminescence spectrum almost perfectly matches the detector spectrum, overlapping from 6.2 μm to 7.1 μm. © *2012 American Institute of Physics*. [http://dx.doi.org/10.1063/1.4767128]

Certainly, semiconductor heterostructures are the key technology for modern photonics. Following the idea of stimulated emission in superlattices by Kazarinov and Suris[1] from 1971 the quantum cascade laser (QCL) was experimentally demonstrated about two decades later by Faist *et al.*[2] Currently, QCLs provide high optical power, wavelength tunability and are one of the most influential devices in mid-infrared and terahertz photonics. Hofstetter *et al.* have reported the use of a QCL as a photovoltaic detector.[3] Although this structure was not optimized for detection, the concept of the quantum cascade detector (QCD) was born. Quantum cascade structures were designed and optimized for infrared and terahertz detection by Graf *et al.*[4,5] and by Gendron *et al.*,[6,7] who introduced the term QCD. QCDs have been fabricated from various material systems, e.g., GaAs/AlGaAs and InGaAs/InAlAs, for mid-infrared and terahertz,[8] as well as InGaAs/AlAsSb[9] and GaN/AlGaN[10] for near-infrared.

QCLs are excellent bright sources for spectroscopic applications such as biological and chemical sensing in gas- and liquid-phases.[11] For spectroscopic sensing, it is desirable to emit spectrally single mode, while covering a broad spectral range. This can be realized with a tunable external cavity[12] or on a single-chip, using a distributed feedback cavity array[13] or a two-dimensional ring cavity surface emitting QCL array.[14] So far, QCLs have been widely used in combination with multipass cells,[15] high-finesse optical cavities,[16] photo-acoustic[17] cells, or hollow fibers.[18] Much effort has been devoted to develop compact systems for mobile chemical fingerprinting,[19] but the ultimate goal of a monolithic integration has not been reached yet. To build a monolithic integrated chemical sensor, it is necessary to generate, manipulate, and detect light on the same chip.

In this letter, we demonstrate design and fabrication of a bi-functional device operating at room-temperature, which detects at the same wavelength as it coherently emits. Our device combines the functionality of a QCL and a QCD within the same active region. By simply changing the applied bias, our device switches between detection/absorption (0 kV/cm), transparency and gain (58 kV/cm).

To understand the challenges, as well as the potential of such a bi-functional device, one has to look into the detailed function of both the QCL and the QCD. In QCLs, electrons are injected from a reservoir, e.g., from a miniband into the upper laser level. The electrons of this upper level are depopulated to the lower laser level via stimulated emission or non-radiative scattering, followed by phonon assisted depopulation via multiple extraction levels. Fast extraction is essential to provide inversion and thus optical gain. The extracted electrons are injected into the upper laser level of the next cascade, e.g., via a miniband. This process is repeated about 20–50 times for mid-infrared QCLs. As photons are generated by intersubband transitions, the emission wavelength is determined by the bandstructure of the cascaded heterostructure and can be engineered to cover a relatively wide range.

QCDs are intersubband detectors based on a cascaded asymmetric quantum well structure that do not require an external bias and thus yield a negligible dark current. Compared to the more commonly used photoconductive quantum well infrared detectors (QWIPs),[20] QCDs are reported to perform better at high temperatures[21] and provide more design freedom using the same material compound. Near thermal equilibrium, most electrons are in the lower detector level (around 70% at room-temperature, assuming a LO-phonon based extractor). If such an electron is optically excited to the upper detector level, it has a finite probability of being extracted before it scatters back to the lower level. Due to the asymmetric design, electrons flow in a preferred direction, when the device is illuminated at the proper wavelength. The electron extraction is commonly realized via resonant tunneling and LO-phonon scattering. Since no external bias is necessary, the high-temperature performance is only limited by Johnson noise (thermal noise) and not by dark current as it is the case for photoconductive QWIPs. As the strength of thermal noise is related to the device resistance, the detectivity can be enhanced by increasing the device resistance.

[a)]Electronic mail: benedikt.schwarz@tuwien.ac.at.

Same-frequency lasing and detection utilizing the identical device structure implies several difficulties. A standard QCL can, in principle, be used as a detector, but will detect at a much shorter wavelength (blue-shift). As illustrated in Figure 1, this shift is because the detector's optical transition occurs between the upper laser level and an extraction level, not the lower laser level. Due to this intrinsic energy-shift and the poor extraction efficiency, it is neither possible to get a good performance nor to match the emission wavelength. The goal for our bi-functional devices is to utilize the function of a QCL and a QCD using the same epilayer. Apart from wavelength matching, such a device has to provide a good injection into the upper level if acting as a laser as well as a good extraction out of the upper level if acting as a detector. If aiming for a bi-functional device, trade-offs have to be found for the design issues of a laser and of a detector.

To design a bi-functional active region, we have developed a software to simultaneously tune the performance for both the laser and the detector. Our quantum cascade device optimizer is based on a highly efficient semi-classical Monte-Carlo transport simulator, which is part of the Vienna Schrödinger Poisson (VSP) framework.[24] Due to the multidimensional optimization problem, a full quantum mechanical approach has far too high computational costs. Therefore, a simulation tool based on non-equilibriums Greens functions (NEGF) is not suitable. The semi-classical Monte-Carlo simulator used in this work is based on the Pauli master equation. Transport is modeled via scattering between energy states, including acoustic and optical deformation potential, polar optical electron-phonon scattering as well as alloy, intervalley, and interface roughness scattering. Our optimizer continuously improves a reference design, by modifying the device layer structure. For this purpose, we represent the layer thicknesses by a vector. A new device is generated by adding a specific vector that is cyclically shifted across the cascaded period. Examples for such vectors are [0.1], [−0.1] or [0.1, 0, 0.1], [−0.1, 0, −0.1], where in the former case one layer is increased or decreased by 0.1 nm and in the latter two adjacent wells or barriers are increased or decreased by 0.1 nm. The modified devices are simulated in parallel on multiple cores for both the laser and the detector operating condition. The device performance is calculated from output quantities, e.g., energy separations, dipole matrix elements, overlap integrals, or optical gain. If a new device performs better, it is used as the reference for the following optimization process. One optimization step takes between ∼5 s and 5 min on one core of a present desktop CPU, depending whether transport and Poisson's equation is included or not.

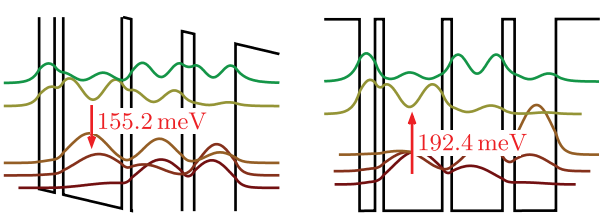

FIG. 1. Using a 4-well active region as a detector leads to an intrinsic energy-shift between the laser and the detector. The detector is blue-shifted, because the optical transition occurs between the lowest extraction level and the upper laser level, not the lower laser level.

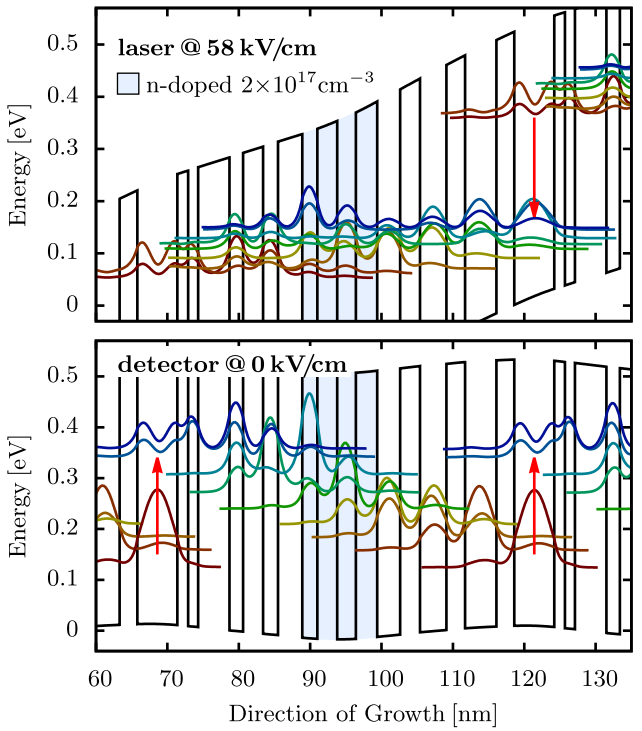

FIG. 2. Bandstructure of the bi-functional active region at laser operation (a) and detector operation (b). The layer sequence of the $In_{0.52}Al_{0.48}As/In_{0.53}Ga_{0.47}As$ structure, starting from the injector barrier, is as follows: **4.4**/1.9/**2.8**/2.1/**3.4**/2.1/**2.8**/2.6/**3.0**/3.2/**2.8**/3.7/**2.6**/4.4/**2.5**/5.6/**1.5**/1.4 nm. The barrier layers are in bold and the underlined layers are n-doped with Si 2×10^{17} cm^{-3}.

The bandstructure of our bi-functional active region is shown in Figure 2. At 58 kV/cm, it acts as a laser, at zero bias as a detector. The intrinsic energy-shift between the laser's and the detector's optical transition (see Figure 1) was compensated by inserting a narrow well between the injector and the active well. If strongly coupled to the active well, it produces a red-shift of the lasing transition compared to the detecting transition, as illustrated in Figure 3. The width of the narrow well is designed, such that its energy level matches the upper level of the active well, which causes the levels to degenerate (levels 2 and 3). The lower degenerated energy level (level 2) is used as the upper level for the laser and the detector. At laser bias the coupling is reduced, because the energy level of the narrow well is shifted towards higher energy. Thus, the detector transition

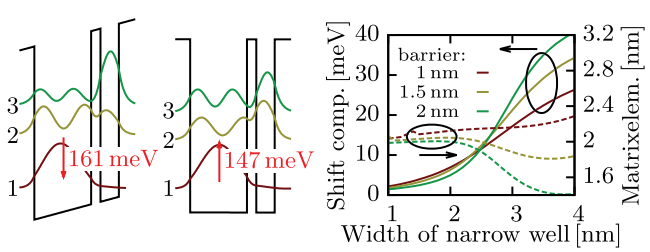

FIG. 3. The intrinsic energy-shift between the laser's and the detector's optical transition is compensated by inserting a narrow well with its energy level strongly coupled to the upper level of the active well. The reduced coupling due to bias results in a red-shift of the detector transition compared to the laser transition. The right plot shows the compensation shift and the detectors dipole matrix element over the width of the narrow well for three different barrier widths.

(between levels 1 and 2) is red-shifted compared to the laser transition. This effect compensates the intrinsic blue-shift between the laser and the detector.

In the case of a 4-well active region, this induced red-shift is still too small to fully compensate the intrinsic blue-shift. The compensating red-shift could be further increased by increasing the width of the narrow well, but the optical transition becomes more and more diagonal, which reduces the dipole matrix element and thus the device performance. We have overcome this problem by first reducing the coupling between the lower laser level and the laser extraction levels to minimize the intrinsic shift, before compensating it. This reduced coupling actually results in a structure similar to the well known bound-to-continuum design.[25] This design allows wavelength matching without significantly reducing the dipole matrix element.

By adjusting the coupling strength between the upper detector level and its extraction level, these levels split up to match the gain peaks of the bound-to-continuum design, as shown in Figure 4. The three uppermost extractor levels of the phonon ladder play a crucial role in both the laser and the detector operation. At zero bias, these three levels are designed to provide efficient extraction via resonant tunneling and LO-phonon scattering. High scattering rates are provided by proper energy separation and optimized overlap integrals. At laser bias, the lowest of these three levels acts as injector level. The other two levels then provide additional tunneling paths to further enhance the extraction of electrons from the lower laser levels.

The other part of the injector/extractor is optimized to provide fast depopulation of the lower level under laser conditions rather than enhancing the detector performance. When designing a pure detector, this part can be used to increase the device resistance with large barriers. However, this reduces the laser performance significantly. To reduce thermal population, which in turn reduces the responsivity at higher temperatures, the separation between the lower detector level and the lowest phonon ladder level was designed to be relatively large.

We have chosen a sheet doping density of $2.1 \times 10^{11}\,\mathrm{cm}^{-2}$, which is a typical value for both QCLs and QCDs. A higher doping would increase the responsivity of the QCD,[22] but evidently would increase the waveguide losses and thus the laser threshold.[23] Although, QCDs are commonly doped in the active well, we put the doping into the injector/extractor, as it is common for lasers. In this case, one has to include Poisson's equation self-consistently.

The device was grown by molecular beam epitaxy (MBE) of slightly strain compensated InGaAs/InAlAs on an n-doped InP substrate (Si, $2 \times 10^{17}\,\mathrm{cm}^{-3}$), with a period mismatch <1%. The waveguide consists of 35 periods of the active region sandwiched between two InGaAs layers, an InAlAs top cladding layer, similar to the optimized waveguide design presented in Ref. 26. The confinement factor and waveguide losses were calculated as 0.64 and $5.54\,\mathrm{cm}^{-1}$. The laser and the detector characteristics were measured from a $10\,\mu\mathrm{m} \times 2\,\mathrm{mm}$ and a $10\,\mu\mathrm{m} \times 0.6\,\mathrm{mm}$ ridge. We were able to achieve room-temperature operation for the detector with a nice overlap to the laser spectrum from 6.4 μm to 6.8 μm. Figure 4 shows the emission spectrum of the laser, the photocurrent spectrum of the detector, as well as the electro-luminescence spectrum measured slightly below laser threshold. The electro-luminescence spectrum almost perfectly matches the detector spectrum. This indicates that our device is capable to emit as well as detect in a broad spectral range from 6.2 μm to 7.1 μm. This is important for chemical sensing applications to distinguish different chemicals with great selectivity and facilitated calibration.[11]

The output power and current-voltage characteristic in laser operation are shown in Figure 5 for different temperatures. Our bi-functional device has a threshold current of $8\,\mathrm{kA/cm}^2$ at room-temperature. The improvement of the device performance, especially the reduction of the threshold current will be a major issue of our future work on bi-functional quantum cascade devices.

Figure 6 shows the detector responsivity at different temperatures. We have observed a peak responsivity of 10 mA/W at 80 K and 3.6 mA/W at 300 K, which in turn is a good value even for a pure QCD.[8] The resistance-area R_0A product, shown in the inset, is essential for the characterization of the noise behavior for Johnson noise limited detectors, as it is the case for QCDs at zero bias and higher temperatures. The detectivity can then be calculated from

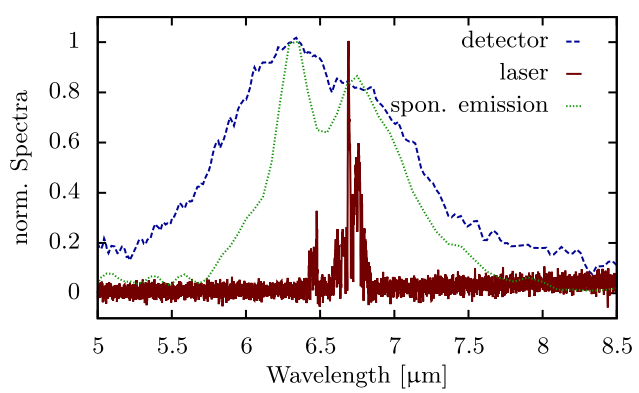

FIG. 4. The measured spectra of the bi-functional active region at room-temperature. Both the laser and the electro-luminescence spectra were measured from a $10\,\mu\mathrm{m} \times 2\,\mathrm{mm}$ ridge with 100 ns pulses at 5 kHz. The two peaks of the electro-luminescence spectrum result from atmospheric absorption. The photocurrent spectra of the detector was measured by focusing the light from a low intensity globar source onto a $10\,\mu\mathrm{m} \times 0.6\,\mathrm{mm}$ ridge facet, normalized by the atmospheric absorption spectrum.

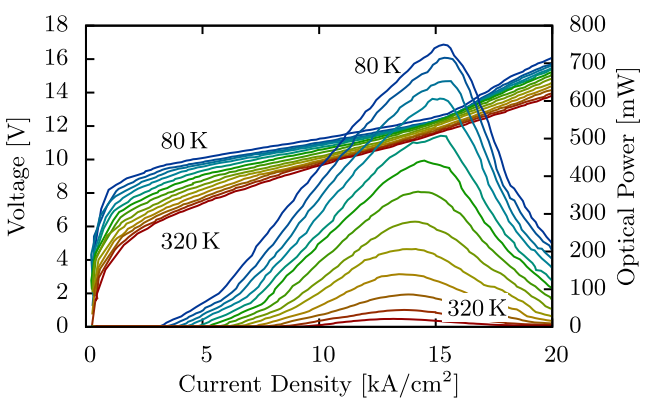

FIG. 5. Optical output power and current-voltage characteristic of the bi-functional device. The curves are measured from a $10\,\mu\mathrm{m} \times 2\,\mathrm{mm}$ ridge laser with 100 ns pulses at 5 kHz. The absolute output power was measured with a calibrated DTGS pyroelectric detector.

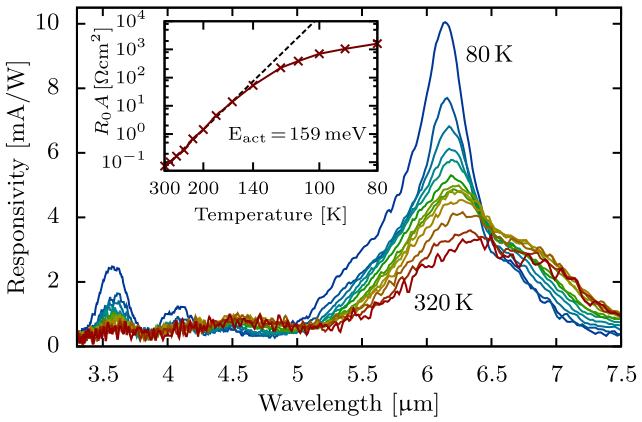

FIG. 6. Spectral responsivity of the detector at different temperatures. The inset shows the resistance-area product R_0A as a function of inverse temperature. The spectra were measured from a 10 μm × 0.6 mm ridge with a FTIR spectrometer, normalized by the atmospheric absorption spectrum. The absolute values were measured with a cw laser adjusted to 10 mW. Considering the measured spot profile and the 5 μm × 10 μm facet, as well as the transmission of the ZnSe cryo-window, we have corrected the laser power for the responsivity calculation to 2.8 mW.

$D_J^* = R\sqrt{\frac{R_0A}{4k_BT}}$, where R is the responsivity, k_B the Boltzmann constant, and T the temperature. This results in a Johnson noise limited detectivity of 2.8×10^9 Jones at 80 K and 6.9×10^6 Jones at 300 K.

In conclusion, we have designed and fabricated a bifunctional quantum cascade device for same-frequency lasing and detection. It utilizes the functionality of a QCL and a QCD to generate, manipulate, and detect light on the same chip with the same epilayer material. We were able to obtain room-temperature operation for both operating conditions. The broad detection and spontaneous emission spectra indicate that our device is capable of emitting and detecting in the spectral range of 6.2 μm and 7.1 μm, using distributed feedback cavities. Therefore, it is a perfect candidate to realize cost effective monolithically integrated chemical and biological sensors based on QCL technology.

The authors acknowledge the support by the Austrian Science Fund, project IRON (F2503-N17), the PLATON project 35 N within the Austrian NANO initiative and the FP7 EU-project ICARUS.

[1]R. F. Kazarinov and R. A. Suris, Sov. Phys. Semicond. **5**, 707 (1971).
[2]J. Faist, F. Capasso, D. L. Sivco, C. Sirtori, A. L. Hutchinson, and A. Y. Cho, Science **264**, 553 (1994).
[3]D. Hofstetter, M. Beck, and J. Faist, Appl. Phys. Lett. **81**, 2683 (2002).
[4]M. Graf, G. Scalari, D. Hofstetter, J. Faist, H. Beere, E. Linfield, D. Ritchie, and G. Davies, Appl. Phys. Lett. **84**, 475 (2004).
[5]M. Graf, N. Hoyler, M. Giovannini, J. Faist, and D. Hofstetter, Appl. Phys. Lett. **88**, 241118 (2006).
[6]L. Gendron, M. Carras, A. Huynh, V. Ortiz, C. Koeniguer, and V. Berger, Appl. Phys. Lett. **85**, 2824 (2004).
[7]L. Gendron, C. Koeniguer, V. Berger, and X. Marcadet, Appl. Phys. Lett. **86**, 121116 (2005).
[8]F. R. Giorgetta, E. Baumann, M. Graf, Y. Quankui, C. Manz, K. Kohler, H. E. Beere, D. Ritchie, E. Linfield, A. G. Davies, Y. Fedoryshyn, H. Jackel, M. Fischer, J. Faist, and D. Hofstetter, IEEE J. Quantum Electron. **45**, 1039 (2009).
[9]F. R. Giorgetta, E. Baumann, D. Hofstetter, C. Manz, Q. Yang, K. Köhler, and M. Graf, Appl. Phys. Lett. **91**, 111115 (2007).
[10]S. Sakr, E. Giraud, A. Dussaigne, M. Tchernycheva, N. Grandjean, and F. H. Julien, Appl. Phys. Lett. **100**, 181103 (2012).
[11]A. A. Kosterev and F. K. Tittel, IEEE J. Quantum Electron. **38**, 582 (2002).
[12]A. Hugi, R. Maulini, and J. Faist, Semicond. Sci. Technol. **25**, 083001 (2010).
[13]B. G. Lee, M. A. Belkin, C. Pflugl, L. Diehl, H. A. Zhang, R. M. Audet, J. MacArthur, D. P. Bour, S. W. Corzine, G. E. Hufler, and F. Capasso, IEEE J. Quantum Electron. **45**, 554 (2009).
[14]E. Mujagi, C. Schwarzer, Y. Yao, J. Chen, C. Gmachl, and G. Strasser, Appl. Phys. Lett. **98**, 141101 (2011).
[15]A. A. Kosterev, R. F. Curl, F. K. Tittel, C. Gmachl, F. Capasso, D. L. Sivco, J. N. Baillargeon, A. L. Hutchinson, and A. Y. Cho, Appl. Opt. **39**, 4425 (2000).
[16]G. Berdena, R. Peetersa, and G. Meijer, Int. Rev. Phys. Chem. **19**, 565 (2000).
[17]D. Hofstetter, M. Beck, J. Faist, M. Nägele, and M. W. Sigrist, Opt. Lett. **26**, 887 (2001).
[18]C. Charlton, F. de Melas, A. Inberg, N. Croitoru, and B. Mizaikoff, IEE Proc.: Optoelectron. **150**, 306 (2003).
[19]S.-S. Kim, C. Young, and B. Mizaikoff, Anal. Bioanal. Chem. **390**, 231 (2008).
[20]H. Schneider and H. C. Liu, *Quantum Well Infrared Photodetectors* (Springer, Berlin, 2006).
[21]A. Gomez, M. Carras, A. Nedelcu, E. Costard, X. Marcadet, and V. Berger, Proc. SPIE **6900**, 69000J (2008).
[22]D. Hofstetter, F. R. Giorgetta, E. Baumann, Q. Yang, C. Manz, and K. Köhler, Appl. Phys. B **100**, 313 (2010).
[23]T. Aellen, M. Beck, N. Hoyler, M. Giovannini, J. Faist, and E. Gini, J. Appl. Phys. **100**, 043101 (2006).
[24]O. Baumgartner, Z. Stanojevic, and H. Kosina, in *IEEE, Proc. of SISPAD* (IEEE, 2011), p. 91.
[25]J. Faist, M. Beck, T. Aellen, and E. Gini, Appl. Phys. Lett. **78**, 147 (2001).
[26]S. S. Howard, Z. Liu, D. Wasserman, A. J. Hoffman, T. S. Ko, and C. F. Gmachl, IEEE J. Sel. Top. Quantum Electron. **13**, 1054 (2007).